Novel Mixed Conducting $SrSc_{0.05}Co_{0.95}O_{3-\delta}$ Ceramic Membrane for Oxygen Separation

Pingying Zeng, Ran Ran, Zhihao Chen, Hongxia Gu, and Zongping Shao
State Key Laboratory of Materials-Oriented Chemical Engineering, College of Chemistry and Chemical Engineering, Nanjing University of Technology, Nanjing, JiangSu 210009, P.R. China

Shaomin Liu
The Australian Research Council (ARC) Center for Functional Nanomaterials, School of Engineering, The University of Queensland, Brisbane QLD 4072, Australia

DOI 10.1002/aic.11334
Published online October 16, 2007 in Wiley InterScience (www.interscience.wiley.com).

A novel perovskite-type mixed-conducting oxide of $SrSc_{0.05}Co_{0.95}O_{3-\delta}$ (SSC) was synthesized by a combined EDTA-citrate complexing method. The 5 mol % of Sc^{3+} doping into the B-site of $SrCoO_{3-\delta}$ (SC) through the sol–gel synthesis effectively stabilized the oxygen vacancy disordered cubic perovskite structure of the oxide, and simultaneously resulted in a substantial increase of the electrical conductivity. The oxide was fabricated into dense ceramic membrane for oxygen separation by pressing/sintering process. The oxygen permeation flux of the SSC membrane and the rate-determination step of the permeation process were investigated between 750 and 900°C. The experimental results demonstrated that SSC is a promising membrane for oxygen separation with ultrahigh permeation fluxes, compared favorably with reported high oxygen semipermeable $Ba_{0.5}Sr_{0.5}Co_{0.8}Fe_{0.2}O_{3-\delta}$ and $SrCo_{0.8}Fe_{0.2}O_{3-\delta}$ membranes under air/helium gradient. At the condition of reduced temperature and low oxygen partial pressure at the sweep side atmosphere, the permeation process was found to be rate-determined mainly by the slow oxygen surface exchange kinetics at the air (feed) side membrane surface based on the single cell oxygen permeation study. The activation energy for the oxygen surface exchange and oxygen bulk diffusion was found to be around 126 kJ mol^{-1} and $\leq$62.1 kJ mol^{-1}, respectively. © 2007 American Institute of Chemical Engineers
AIChE J, 53: 3116–3124, 2007
Keywords: oxygen separation, perovskite, mixed conducting, $SrSc_{0.05}Co_{0.95}O_{3-\delta}$, ceramic membrane

Introduction

Oxygen is one of the most important chemicals in the world. Many industrial processes and other special fields like military, aerospace, and medical applications, require oxygen or oxygen-enriched streams. Oxygen is normally obtained from air by one of the three conventional processes: the distillation of cryogenic air (for large scale production), pressure swing adsorption, and vacuum swing adsorption (for application requiring oxygen purities <93%). The cost of the process depends strongly on the required purity and the production scale. On the other hand, some composite oxides with defined structure, like perovskite, have mixed oxygen ionic and electronic conductivity at high temperature.[1–3] The ce-

Correspondence concerning this article should be addressed to Z. Shao at shaozp@njut.edu.cn.

ramic membranes made from such materials allow oxygen to permeate through with infinite oxygen selectivity under the driven of oxygen partial pressure difference across the membrane.[4–8] Such membranes have several potential applications including: pure oxygen production, partial oxidation of methane to syngas, oxidative coupling of hydrocarbon to value-added products, and oxygen-enriched combustion, and so on.[4–15] As compared with the traditional oxygen separation process, such as the distillation of cryogenic air, the advantages of ceramic membrane process are obvious: simple in operation, substantially reduction in capital cost both for plant construction and the daily operation, and capable of coupling reaction.

The oxygen permeation flux is one of the most important parameters that usually have been first considered in the development of new materials for commercial application purposes.[16,17] However, for most of the materials developed up to now, their oxygen permeability is still too low to be commercially considered.[18–20] High permeation flux means more compact of the reactor system; therefore a reduction in capital cost for the reactor construction can be envisaged. Additional benefit of high permeation flux is the effective protection of the membrane from reduction during the coupling reaction.[21,22] The high permeation flux ensures a sufficient oxygen supply from the high oxygen partial pressure side atmosphere (air side) to form a protecting oxygen layer on the membrane surface at the sweep side, thus suppressing the consumption of the lattice oxygen of the membrane material by the reducing atmosphere.[21] The development of new membrane materials with high oxygen permeability and phase/chemical stability is critical in accelerating the industrial scale application of mixed conducting membrane.

The oxygen permeability of the membrane is strongly dependent on the material structure and composition.[23–28] Compared with other phase structures like fluorite[23,24] and K_2NiF_4,[25] the perovskite membranes displays much higher oxygen permeability with favorable phase/chemical stability.[26–28] The perovskite is a group of oxides with a general structure of ABO_3. The BO_3 atoms form the framework of interconnected octahedral with B ion at the corners. Elements for the A sites can be chosen from cerium, calcium, barium, strontium, or various rare earth metals to form 12 coordination with adjacent oxygen ions. The B site can be occupied by cobalt, iron, or other transition metal ions. The advantages of perovskite as oxygen separation membrane material lie on its compositional versatility, high electrical conductivity, and favorable structural and phase stability. More than 90% of the metal elements in periodic table can be doped to form a stable perovskite structure. Some perovskites can be strategically formulated to simultaneously possess high electronic and oxygen ionic conductivities, which ensure the high oxygen permeability.[29,30]

Earlier, we reported the influence of Sc^{3+} doping in the B-site of $SrCoO_{3-\delta}$ on its lattice structure/phase stability, electrical conductivity, and cathode performance for intermediate-temperature solid-oxide fuel cells.[31] It was found that $SrCoO_{3-\delta}$ doped by 5 mol % of Sc^{3+} resulted in a very stable cubic perovskite structure and the highest electrical conductivity. In this article, we further investigated the potential of using this new perovskite as a mixed conducting ceramic membrane for air separation. The membrane was prepared by a combined dry pressing and sintering method. Oxygen permeation was studied by exposing the membrane under air/helium gradient. For a more in-depth understanding, the rate-determination steps for oxygen transport process were clarified by theoretical and experimental investigation.

Experimental

$SrCoO_{3-\delta}$ (SC) and $SrSc_{0.05}Co_{0.95}O_{3-\delta}$ (SSC) oxides were synthesized by a combined EDTA-citrate complexing sol–gel process. $Sr(NO_3)_2$, $Co(NO_3)_2{\cdot}xH_2O$, and Sc_2O_3 (all in A.R. grade) were applied as the raw materials for the metal-ion sources.[31] For a typical synthesis, 0.2689 g Sc_2O_3 powder was first dissolved in 0.82 mL HNO_3 (14.50 mol L^{-1}) solution at 90°C under stirring. The as-obtained $Sc(NO_3)_3$ solution and 16.5072 g $Sr(NO_3)_2$ and 88.44 mL $Co(NO_3)_2$ (0.8379 mol L^{-1}) were mixed with 90 mL deionized water to obtain a mixed solution under stirring. 45.56 g EDTA acid powder was dissolved in 117 mL $NH_3{\cdot}H_2O$ (13.33 mol L^{-1}) solution at a parallel experiment, which was then added to the mixed solution, followed by the addition of 65.64 g citric acid. $NH_3{\cdot}H_2O$ was used to maintain the pH value of the system at ~6. Under stirring and gentle heating at 90°C, a clear pink colored solution was obtained. A viscous gel was finally obtained with the evaporation of the water. The gel was pretreated at 250°C for primary decomposition and the formation of a gray solid precursor, which was then fired at various temperatures in air for 5 h to result in the final product of SSC. The powder calcined at 900°C was pressed into disk-shape green membranes with a diameter of 15 mm, which were then sintered into dense membranes at 1100°C for 5 h under stagnant air. The sintered membranes had a diameter of 12–13 mm and thickness of 0.7–1.5 mm.

The phase structure of the samples was investigated using a Bruker D8 Advance diffractometer with Cu Kα radiation. The experimental diffraction patterns were collected at room temperature by step scanning in the range of $10° \leq \theta \leq 90°$.

The electrical conductivity was measured by the four-probe DC method on sintered bars under air upon cooling from 900 to 300°C, 5°C per step. Silver paste was painted on the bar edges (separated by a distance L) to form current and voltage electrodes. Two silver wires acted as current contacts while the other two sliver wires acted as the voltage contacts, which were attached to the electrodes using silver paste. The sample was placed in a vertical split tube furnace. A constant current was applied to the two current wires and the voltage response on the two voltage wires were recorded using a Keithley 2420 source meter. The current was increased from 1 μA to a maximum value of 2A.

Symmetric cell configuration was used for the determination of the activation energy for oxygen surface exchange over SSC membrane. Two nominally identical SSC cathodes (1.21 cm^2) were deposited on each side of the $Sm_{0.15}Ce_{0.85}O_{1.925}$ electrolyte pellet by painting technique and calcined at 1000°C for 5 h under static air atmosphere. Impedance measurements were performed using an electrochemical workstation based on Solartron 1260A frequency response analyzer together with a 1287 Potentiostat/Galvanostat. The two-electrode cells were tested under air at open circuit volt-

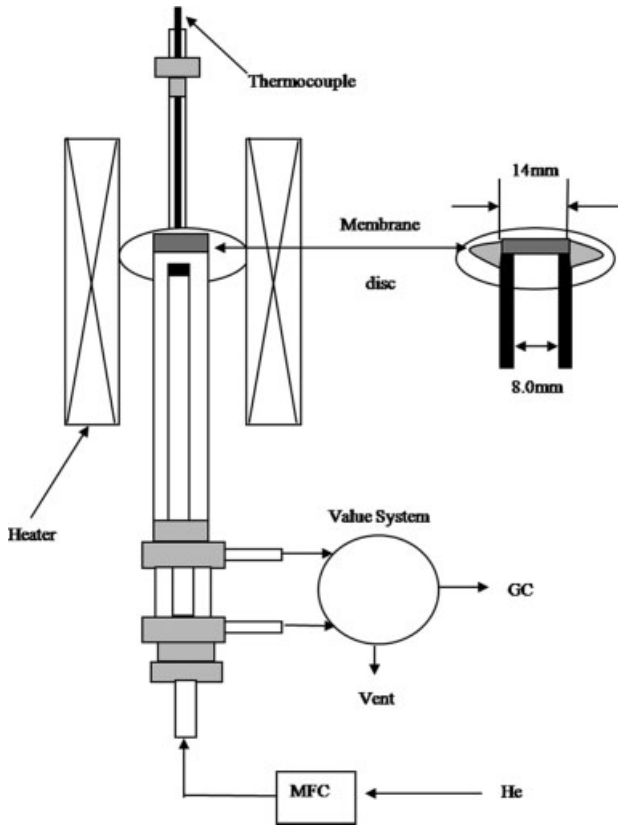

Figure 1. The diagram of the set-up for the oxygen permeation measurement.

age with the frequency range of 0.1–10^5 Hz and applied AC voltage amplitude of 10 mV.

Permeation properties of the membranes were investigated using a high-temperature oxygen permeation cell as shown in Figure 1. Silver paste was used as the sealant to seal the membrane disk onto a dense quartz tube. An inner surface area of around 0.45 cm^2 was exposed for permeation study. The sidewall of the membrane disk was also covered with the silver paste to avoid radial contribution to the oxygen permeation flux. Helium was used as the sweep gas to carry the permeated oxygen to a Varian 3800 gas chromatography (GC) equipped with a 5 Å molecular sieve capillary column for in-situ gas composition analysis. Helium also acted as the diluted gas to create the oxygen partial pressure gradient across the membrane. Helium flowrates were controlled by D07-19/ZM Mass Flow Controller and D08-8C/ZM Flow Integrator (with an accuracy of ± 2 mL/min). The detection limit of oxygen permeation flux by GC was 0.004 mL/(min cm^2), values lower than which will be became undetectable.

Results and Discussion

Figure 2 shows the room-temperature X-ray diffraction patterns of SC and SSC powders prepared by calcination of the sol–gel precursors at 1000°C for 5 h under air atmosphere. SC oxide demonstrates the typical 2-H hexagonal perovskite, while SSC displays the pure phase cubic perovskite structure. It suggests that the small amount of Sc^{3+} (5 mol %) doping into the B-site of SC effectively stabilized the cubic perovskite phase. Depending on the operating temperature, oxygen partial pressure of the environment, thermal history, and synthesis methods, SC can take several crystal structures: 2H-type hexagonal perovskite, oxygen vacancy-ordered brownmillerite, rhombohedral perovskite, or cubic perovskite structure. However, only the cubic perovskite is the oxygen vacancy disordered structure giving the best oxygen permeability. Under the oxygen permeation condition, the SC membrane may experience a large oxygen partial pressure gradient and complicated thermal environment/history. Therefore the phase transition may be accompanied during the operation,[32] which is highly detrimental to the integration of the membrane because a large dimensional change may be accompanied, which can lead to the failure of the membrane reactor. The cubic structure of SSC was found to be stable from room temperature to high temperature under oxygen, air or argon atmosphere.[31] It therefore suggests the effectiveness of the small amount of Sc^{3+} to stabilize the cubic perovskite of SC phase.

The electrical conductivity of SC and SSC was measured by the four-probe DC method under pure oxygen, air or argon atmosphere, and the results are shown in Figure 3. The 2H-type hexagonal perovskite structured SC shows relative lower conductivity. A value of only ~4 S cm^{-1} was observed at 300°C under air atmosphere. With the increase of the operation temperature, the conductivity increased steadily and reached a value of 24 S cm^{-1} at 900°C. The slight enhancement of electrical conductivity with the increase of oxygen partial pressure in the atmosphere indicates the P-type conducting mechanism. However, the small amount of Sc^{3+} (5 mol %) doping into the lattice structure of SC, i.e., the formation of SSC resulted in the substantial increase of the electrical conductivity, which reached about 140 S cm^{-1} at 300°C under air. SSC showed the semiconductor behavior at the relatively low operation temperature, characterized by the increase of the conductivity with the increase of operation temperature, until it reached a maximum value of ~176 S cm^{-1} at ~410°C. With the further increase of the operation temperature, the electrical conduc-

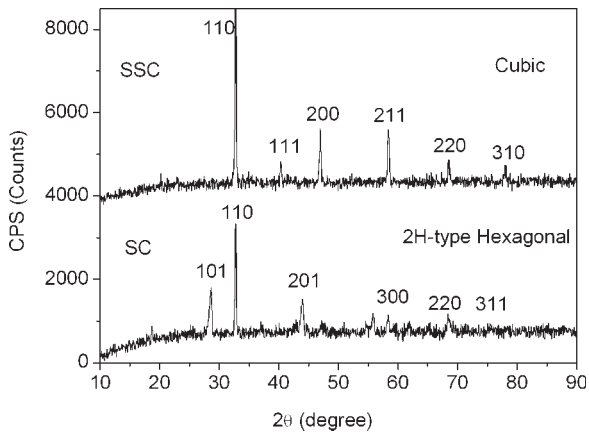

Figure 2. Room-temperature X-ray diffraction patterns of SC and SSC powders calcined at 1000°C.

The index of SC and SSC was based on the 2H-type hexagonal and cubic perovskite structure, respectively.

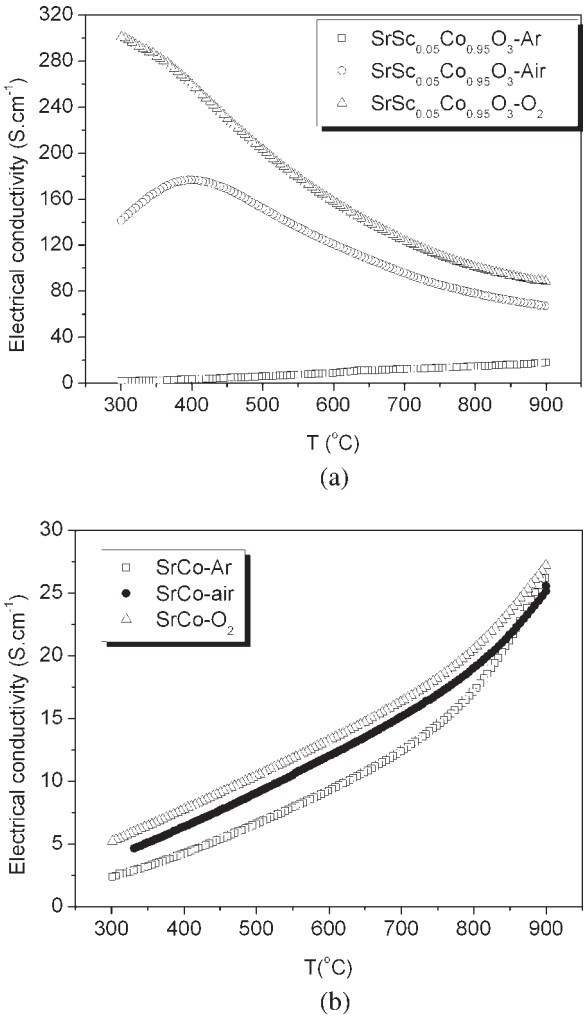

Figure 3. A comparison of the temperature dependence of the conductivity of SSC and SC under air.

tivity of SSC started to show the metal-like behavior, i.e., the decrease of the electrical conductivity with the increase of the operation temperature. However, the conductivity of SSC still reached 70 S cm^{-1} at 900°C, which was about three times that of the SC at the same condition.

It is suggested that the electronic conduction was created via the overlapping of the oxygen 2P orbital with the transition metal 3D orbital through a mechanism named as the Zerner double exchange process as shown below[33]:

$$B^{n+} - O^{2-} - B^{(n+1)+} \Rightarrow B^{(n+1)+} - O^{-} - B^{(n+1)+}$$
$$\Rightarrow B^{(n+1)+} - O^{2-} - B^{n+}$$

In the cubic perovskite phase, the angle of the B—O—B bond is 180°, most favorable for the electronic conduction because of the complete orbital overlapping. On the other hand, the cubic perovskite also allows the highest degree of freedom for oxide ion and electron to transport due to the highest symmetric mobility for the 3D; therefore, it also promotes the maximum oxygen ionic conductivity.

For the ceramic membranes with mixed oxygen ionic and electronic conductivity, when the permeation process is controlled by the bulk diffusion, the oxygen permeation flux can be expressed by Eq. 1:

$$J_{O_2} = -\frac{RT}{4^2F^2L} \cdot \int_{\ln P''^{S}_{O_2}}^{\ln P''^{S}_{O_2}} \frac{\sigma_{ion} \cdot \sigma_e}{\sigma_{ion} + \sigma_e} \cdot d[\ln P_{O_2}] \quad (1)$$

$P''^{S}_{O_2}$, $P''^{S}_{O_2}$ are the oxygen partial pressures at the feed side membrane surface and sweep side membrane surface, respectively, σ_{ion} and σ_e are the oxygen ionic and electronic conductivity, respectively, L is the thickness of the membrane. The increase of both electronic and oxygen ionic conductivity suggests that a much higher oxygen permeation flux could be achieved for membrane based on SSC as compared with that of its parent compound SC.

Disk-shaped membranes from SSC perovskite oxide were employed for oxygen permeation study. Figure 4 shows the typical SEM morphologies of the SSC membranes after sintering the green membranes at 1100°C in air for 5 h. It clearly shows that the resulted membranes were well sintered with small amount of closed holes trapped inside the membranes. No connected pores penetrated the membrane was observed from the SEM of the crosssectional view of the pellet. The gas tightness was confirmed by the gas leaking test detected by the GC method at room temperature. The relative density is higher than 95% as measured by the Archimedes method using water as media. The sintered membrane does not have a distinguished grain boundary, especially at the cross section. This is very different from that of $Ba_{0.5}Sr_{0.5}Co_{0.8}Fe_{0.2}O_{3-\delta}$ (BSCF)[4] or $La_{0.6}Sr_{0.4}Co_{0.8}Fe_{0.2}O_{3-\delta}$ (LSCF)[34] membranes sintered at similar conditions. The estimated grain size for the 1100°C sintered SSC membrane is 4–10 μm.

The obtained membranes were sealed with Ag paste onto the top of quartz tubes. The reactor was slowly heated to 950°C and maintained at 950°C for half hour to soften the Ag seals. The softened Ag provided the required sealing. The membrane was cooled down to 900°C, followed by the introduction of the sweep gas of helium to create an oxygen partial pressure gradient across the membrane. A net oxygen flux permeated from the air side to the sweep side was immediately observed. The oxygen flux resulted in the increase of the oxygen partial pressure at the sweep side, which reversely led to the decrease of oxygen permeation rate until a steady permeation flux was reached. Figure 5 shows the steady state oxygen permeation fluxes of SSC at constant helium sweep rate of 100 mL min^{-1} [STP] and oxygen partial pressure of the sweep side atmosphere (P''_{O_2}) of 0.014 atm. A quite high oxygen permeation flux was observed, which is comparable with that of the high-permeable perovskite BSCF[4,21,35] and $SrCo_{0.8}Fe_{0.2}O_{3-\delta}$[1,35,36] membranes under the similar operation conditions. For example, a permeation flux as high as 3.1 $mL \cdot cm^{-2} \cdot min^{-1}$ [STP] was reached at 900°C; and even at 675°C, the oxygen flux still arrived at about 0.26 $mL \cdot cm^{-2} \cdot min^{-1}$. On the contrary, the SC membrane before the phase transition from 2-H hexagonal structure to perovskite showed negligible permeation flux.[32] The significant higher permeation fluxes of SSC as compared

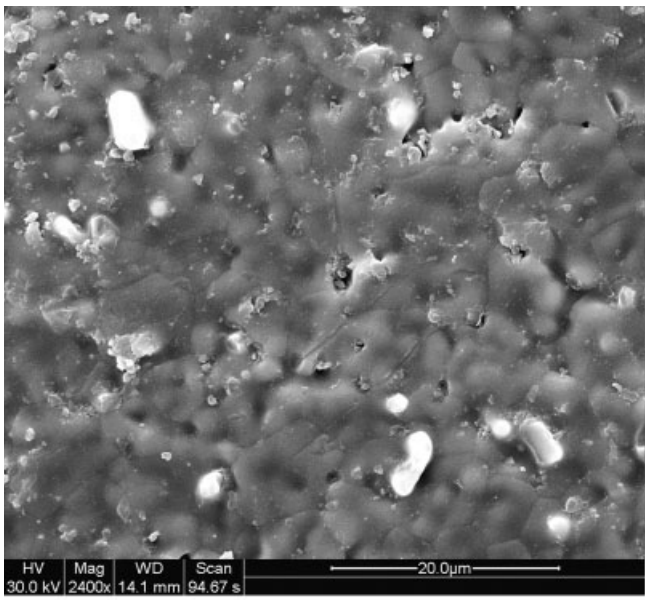

(a)

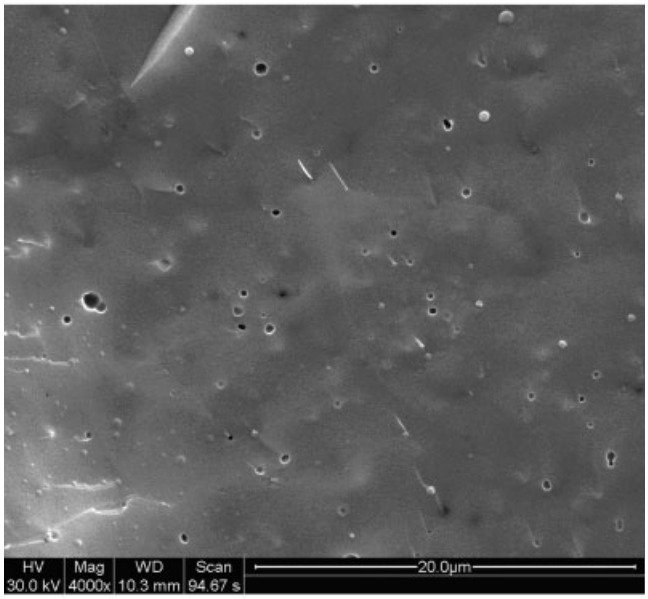

(b)

Figure 4. SEM morphologies of the SSC membranes after sintered of the green membranes at 1100°C for 5 h under air.

(a) Surface section, (b) cross section.

with that of SC membrane demonstrated the importance and effectiveness of the strategic doping of small amount of Sc^{3+} in promoting the oxygen permeability of the oxides. In connection with the XRD and the electrical conductivity results, the higher oxygen permeation rate can be attributed to the successful transformation of the oxygen vacancy ordered 2H-type hexagonal structure to the much more conductive oxygen vacancy disordered cubic perovskite structure.

For the oxygen permeation through a dense ceramic membrane composed of the mixed oxygen ionic and electronic conducting oxide, the oxygen surface exchange rates at either or both sides of the membrane surface(s) and the oxygen vacancy bulk diffusion process may all have important impacts on the oxygen permeation fluxes. Each of them or a combination could be the rate-determination step for the oxygen permeation. If the permeation process is mainly rate-determined by the slow oxygen bulk diffusion process, the thin membrane technology can be applied to increase the permeation flux. However, if the permeation process is mainly rate-determined by the slow oxygen surface exchange kinetics, the further decrease in the membrane thickness would have no obvious effect on the improvement of the flux. Instead, a modification of the surface properties will be of great help. Therefore, recognition of the rate-determination step of the oxygen permeation process is of practical importance. Typically, the investigation of oxygen permeation fluxes through membranes with different thicknesses is applied to determine the rate-determination step in oxygen permeation process. However, it was very difficult to ensure that these membranes with different thickness have identical surface morphologies and bulk properties. The use of improper membranes could lead to misleading conclusions. Furthermore, it is not able to distinguish which surface exchange reaction is the rate determination step simply by varying the membrane thickness. The determination of the rate-limiting step of oxygen permeation process from the single cell permeation measurement then has intrinsic advantages.

For the ceramic membrane with mixed oxygen ionic and electronic conductivity, the permeation flux through the membranes under the driving force of chemical potential differential could be expressed by Eqs. 2 and 3[37]:

$$J_{O_2} = \frac{I_{O_2}}{4F} \tag{2}$$

$$I_{O_2} = \frac{E}{R_{S1} + R_b + R_{S2}} = \frac{E_{S1}}{R_{S1}} = \frac{E_b}{R_b} = \frac{E_{S2}}{R_{S2}} \tag{3}$$

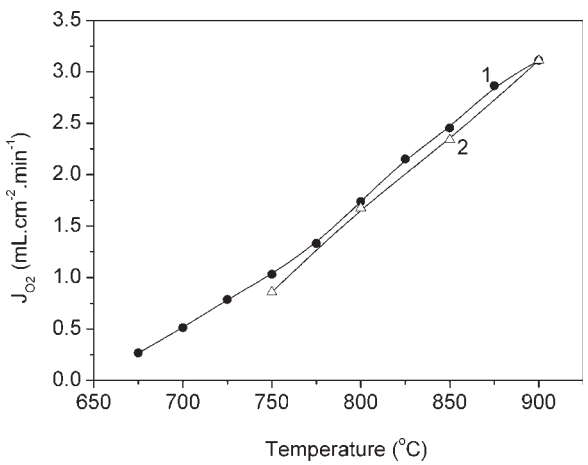

Figure 5. The steady state oxygen permeation fluxes of SSC membrane at constant helium sweep rate of 100 mL min^{-1} [STP] (Curve 1) and at constant oxygen partial pressure of the sweep side atmosphere (P''_{O_2}) of 0.014 atm (Curve 2).

where I_{O2} is the current density; E_{S1}, E_{S2}, E_b, the chemical potentials inputted at the surface of high oxygen partial pressure, the low oxygen partial pressure and the bulk, respectively; R_{S1}, R_{S2}, and R_b, the resistances to surface oxygen exchange at high oxygen partial pressure side ($S1$), at the low oxygen partial pressure side ($S2$), and the resistance to oxygen bulk diffusion, respectively.

The chemical potentials inputted at the surfaces and bulk are:

$$E_{S1} = \frac{\mathrm{RT}}{4F} \cdot \ln \frac{P'_{\mathrm{O}_2}}{P'^{S}_{\mathrm{O}_2}} \tag{4}$$

$$E_{S2} = \frac{\mathrm{RT}}{4F} \cdot \ln \frac{P''^{S}_{\mathrm{O}_2}}{P''_{\mathrm{o}_2}} \tag{5}$$

$$E_b = \frac{\mathrm{RT}}{4F} \cdot \ln \frac{P'^{S}_{\mathrm{O}_2}}{P''^{S}_{\mathrm{O}_2}} \tag{6}$$

where P'_{O_2}, P''_{O_2}, $P'^{S}_{\mathrm{O}_2}$, $P''^{S}_{\mathrm{O}_2}$ are the oxygen partial pressures at the oxygen feed side atmosphere, sweep side atmosphere, feed side membrane surface, and sweep side membrane surface, respectively.

The resistance to oxygen surface exchange can be calculated based on Eq. 7.[38]

$$R_s = \frac{\mathrm{RT}}{S4^2F^2K} \cdot \frac{1}{3/V_{\mathrm{m}} - [V_{\mathrm{O}}^{\mathrm{oo}}]_s} \tag{7}$$

where S is the membrane surface area, K the surface exchange coefficient, V_{m} the mole volume of the oxide, and $[V_{\mathrm{O}}^{\mathrm{oo}}]_{\mathrm{s}}$ the oxygen vacancy concentration at the surface.

The oxygen vacancy concentration can be related with the oxygen ionic conductivity by[9]:

$$\sigma_{\mathrm{ion}} = \frac{4F^2[V_{\mathrm{O}}^{\mathrm{oo}}]D_{\mathrm{v}}}{\mathrm{RTV_m}} \tag{8}$$

where D_{v} is the oxygen diffusion coefficient, and σ_{ion} the oxygen ionic conductivity.

The oxygen ionic conductivity can be further related with the oxygen partial pressure by the empirical equation[39]:

$$\sigma_{\mathrm{ion}} = -\sigma^{\mathrm{o}}_{\mathrm{ion}} \cdot P^{-n}_{\mathrm{O}_2} \tag{9}$$

$\sigma^{o}_{\mathrm{ion}}$ is the oxygen ionic conductivity of the material at the standard condition.

Combining (7), (8), and (9) gives

$$R_s = \frac{\mathrm{RT}}{S4^2F^2K} \cdot \frac{1}{\frac{3}{V_{\mathrm{m}}} - \frac{\sigma^{\mathrm{o}}_{\mathrm{ion}}\mathrm{RTV_m}}{4F^2D_{\mathrm{v}}} \cdot (P^{s}_{\mathrm{O}_2})^{-n}} \tag{10}$$

The oxygen permeation flux for the SSC membrane can be calculated based on any of the following three equations:

$$J_{\mathrm{O}_2} = S \cdot K \cdot \ln \frac{P'_{\mathrm{O}_2}}{P'^{S}_{\mathrm{O}_2}} \cdot \left(\frac{3}{V_m} - \frac{\sigma^{o}_{\mathrm{ion}} \cdot (P'^{S}_{\mathrm{O}_2})^{-n} \cdot \mathrm{RTV_m}}{4F^2D_v} \right) \tag{11}$$

$$J_{\mathrm{O}_2} = S \cdot K \cdot \ln \frac{P'_{\mathrm{O}_2}}{P''_{\mathrm{O}_2}} \cdot \left(\frac{3}{V_{\mathrm{m}}} - \frac{\sigma^{\mathrm{o}}_{\mathrm{ion}} \cdot (P''^{S}_{\mathrm{O}_2})^{-n} \cdot \mathrm{RTV_m}}{4F^2D_{\mathrm{v}}} \right) \tag{12}$$

$$J_{\mathrm{O}_2} = -\frac{\mathrm{RT}}{4^2F^2L} \cdot \int_{\ln P'^{S}_{\mathrm{O}_2}}^{\ln P''^{S}_{\mathrm{O}_2}} \sigma_{\mathrm{ion}}\, d\ln P_{\mathrm{O}_2} = a\left[(P''^{S}_{\mathrm{o}_2})^{-n} - (P'^{S}_{\mathrm{O}_2})^{-n} \right] \tag{13}$$

where

$$a = -\sigma^{\mathrm{o}}_{\mathrm{ion}} \cdot \mathrm{RT}/4^2F^2n \tag{14}$$

When the permeation process is rate-limited by the slow oxygen surface exchange at the feed side membrane surface, the permeation flux can be expressed by:

$$J_{\mathrm{O}_2} = S \cdot K \cdot \ln \frac{P'_{\mathrm{O}_2}}{P''_{\mathrm{O}_2}} \cdot \left(\frac{3}{V_{\mathrm{m}}} - \frac{\sigma^{\mathrm{o}}_{\mathrm{ion}} \cdot (P''_{\mathrm{O}_2})^{-n} \cdot \mathrm{RTV_m}}{4F^2D_{\mathrm{v}}} \right) \tag{15}$$

If it is rate limited by the slow oxygen surface exchange of the sweep side membrane surface, the permeation flux can be expressed by:

$$J_{\mathrm{O}_2} = S \cdot K \cdot \ln \frac{P'_{\mathrm{O}_2}}{P''_{\mathrm{O}_2}} \cdot \left(\frac{3}{V_{\mathrm{m}}} - \frac{\sigma^{\mathrm{o}}_{\mathrm{ion}} \cdot (P'_{\mathrm{O}_2})^{-n} \cdot \mathrm{RTV_m}}{4F^2D_{\mathrm{v}}} \right) \tag{16}$$

Under the slow bulk oxygen diffusion controlling of the permeation process and with overwhelming electronic conductivity of the oxide, the permeation flux can be rewritten as Eq. 17.

$$J_{\mathrm{O}_2} = -\frac{\mathrm{RT}}{4^2F^2L} \cdot \int_{\ln P'_{\mathrm{O}_2}}^{\ln P''_{\mathrm{O}_2}} \sigma_{\mathrm{ion}} \cdot d\ln[P_{\mathrm{O}_2}] = a[(P''_{\mathrm{O}_2})^{-n} - (P'_{\mathrm{O}_2})^{-n}] \tag{17}$$

Based on Eq. 17, at fixed P'_{O_2}, $J_{\mathrm{o}2}$ should increase with the decrease of P''_{O_2} when the permeation process is rate-determined by the slow oxygen bulk diffusion. However, if the permeation process is rate-limited by the slow surface exchange kinetics at the feed side membrane surface, according to Eq. 15, the decrease of P''_{O_2} would have two opposite effects on the permeation flux at the fixed P'_{O_2}. The increase of $\ln \frac{P'_{\mathrm{O}_2}}{P''_{\mathrm{O}_2}}$ would lead to the increase of the permeation flux, while the decrease of $\left[\frac{3}{V_{\mathrm{m}}} - \sigma^{\mathrm{o}}_{\mathrm{ion}} \cdot (P''_{\mathrm{O}_2})^{-n} \cdot RTV_{\mathrm{m}} \right]$ with the decrease of P''_{O_2} would lead to the decrease of the permeation flux. As a whole, $J_{\mathrm{o}2}$ could increase or decrease with the decrease of P''_{O_2}, depending on the relative importance of $\ln \frac{P'_{\mathrm{O}_2}}{P''_{\mathrm{O}_2}}$ and $\left[\frac{3}{V_{\mathrm{m}}} - \sigma^{\mathrm{o}}_{\mathrm{ion}} \cdot (P''_{\mathrm{O}_2})^{-n} \cdot RTV_{\mathrm{m}} \right]$ on the permeation flux. A decrease or constant of $J_{\mathrm{O}2}$ with the decrease of P''_{O_2} strongly suggests that the oxygen permeation process is mainly rate-determined by the slow oxygen exchange at the

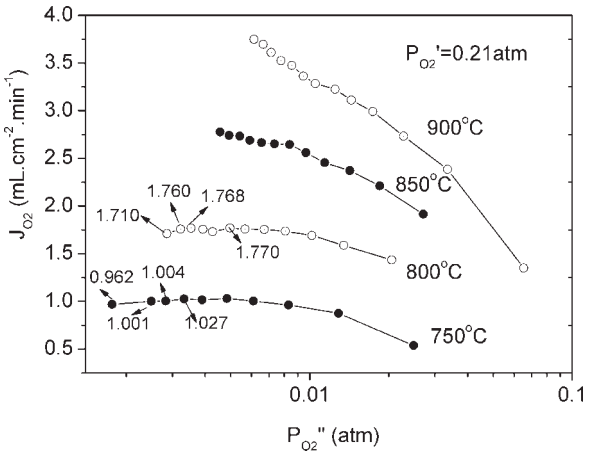

Figure 6. The P''_{O_2} dependence on the oxygen permeation fluxes though SSC membrane at various temperatures with ambient air applied as the feed side atmosphere and varied P''_{O_2} created by the changing of the helium sweep rate.

air side membrane surface. If the permeation process was totally rate-determined by the slow oxygen exchange at the sweep side membrane surface, the permeation flux would increase with the decrease of P''_{O_2}. More specifically, the permeation flux would be proportionally to the value of $\ln\frac{P'_{O_2}}{P''_{O_2}}$.

Figure 6 shows the P''_{O_2} dependence of the oxygen permeation fluxes through SSC membrane at various temperatures with ambient air applied as the feed side atmosphere and varied P''_{O_2} by the changing of the helium sweep rate. It was found that the permeation flux increased with the decrease of P''_{O_2} within the investigated oxygen partial pressure range from 0.005 to 0.065 atm at 900°C, and 0.026 to 0.005 atm at 850°C. However, at the temperature of 800 and 750°C, the permeation flux first increased with the decrease of P''_{O_2} and then decreased. For example, at 800°C, the permeation flux increased with the decrease of P''_{O_2} within the P''_{O_2} range of 0.002 to 0.004 atm, and then decreased with the further decrease of P''_{O_2}. Based on above modeling, the decrease of P''_{O_2} led to the increasing importance of surface exchange in the rate determination of the oxygen permeation process. Therefore, the decrease of oxygen permeation flux with the decrease of P''_{O_2} at 750 and 800°C at relatively lower oxygen partial pressure strongly suggests that the permeation rate was mainly rate-determined by the slow surface exchange kinetics at the feed side membrane surface.

It is well known that the activation energy (E_a) for oxygen surface exchange and bulk diffusion may differ significantly from each other. The occurrence of rate determination of the oxygen permeation process by the slow surface oxygen exchange at the relatively low operation temperature strongly suggests that the oxygen surface exchange kinetics had higher activation energy than that for the oxygen bulk diffusion. The impedance spectroscopy can be used to learn the information of the surface exchange process. For the oxygen reduction over mixed conducting cathode, oxygen was first adsorbed on the cathode surface and dissociated into oxygen ion, which was then incorporated into the bulk of the cathode or diffused along the cathode surface to the electrolyte-cathode interface. Finally the oxygen ion was diffused into the electrolyte layer. The impedance spectroscopy can get the information of the resistance to the oxygen surface reduction and the oxygen transport within the bulk of electrode. Different shapes of the impedance spectroscopy should be observed for the surface exchange kinetics or the bulk oxygen diffusion as a limiting step in the oxygen reduction process.[40] Figure 7 shows the typical impedance spectroscopy of the SSC as the cathode for SDC electrolyte. The symmetric shape of the impedance spectroscopy suggests the oxygen reduction over the SSC cathode was mainly rate-limited by the slow oxygen surface exchange process, coincided with the fact of thin layer of the cathode (10 μm) and the high ionic conductivity of SSC. Therefore, the activation energy (E_a) derived based the temperature dependence of area specific resistance, measured by the symmetric cell configuration, reflected the E_a for the oxygen surface change, which was found to be about 126 kJ mol^{-1} on the basis of Figure 7. The E_a for oxygen permeation derived from the 1000/T dependence of log J_{O2} is the apparent E_a which combines oxygen surface exchange and oxygen bulk diffusion proc-

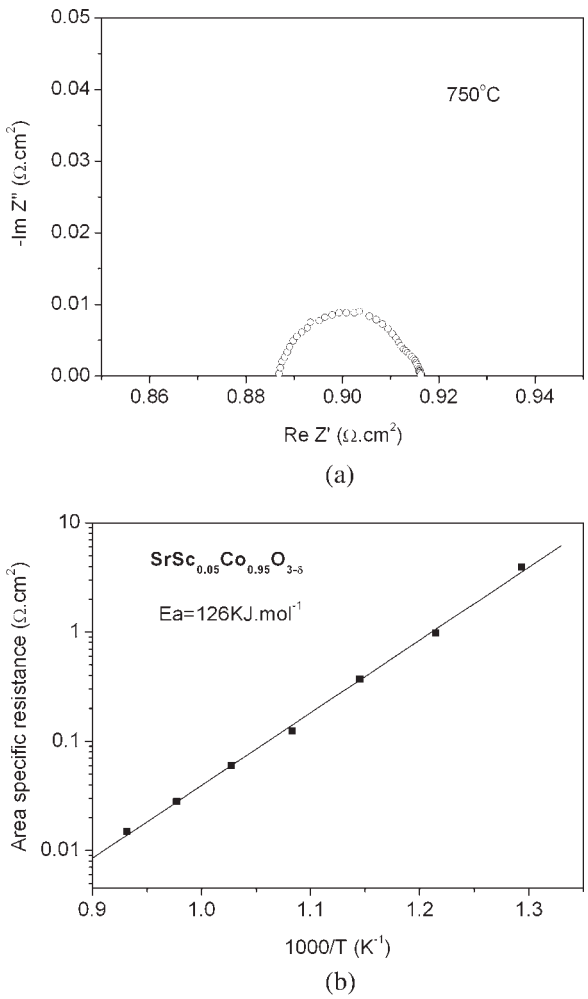

Figure 7. The impedance spectroscopy of the SSC as the cathode for SDC electrolyte.

Table 1. Activation Energy for Oxygen Permeation Through $SrSc_{0.05}Co_{0.95}O_{3-\delta}$ Membrane

Temperature	750°C	800°C	850°C	900°C
750°C	–	122.0 kJ mol^{-1}	96.1 kJ mol^{-1}	84.3 kJ mol^{-1}
800°C	–	–	66.8 kJ mol^{-1}	65.0 kJ mol^{-1}
850°C	–	–	–	62.1 kJ mol^{-1}

d = 0.91 mm, p'_{O_2} = 0.21 atm, and p''_{O_2} = 0.0144 atm.

esses. Table 1 shows the E_a for oxygen permeation through SSC membrane at different temperature zone at the constant P'_{O_2} of 0.21 atm and P''_{O_2} of 0.014 atm. The apparent Ea is found to increase with the decrease of the investigated operation temperature zone. Within the temperature zone of 750–800°C, the E_a for oxygen permeation is found to be around 122 kJ mol^{-1}, which is close to the value of the activation energy for the oxygen surface exchange process (126 kJ mol^{-1}). In connection with the results of Figure 6, we can conclude that the oxygen permeation process at 750–800°C was mainly rate determined by the slow surface exchange kinetics at the air side membrane surface. Because of the higher E_a of the oxygen surface exchange than the oxygen bulk diffusion, the surface exchange kinetics increase more quickly than the oxygen bulk diffusion with the increase of operation temperature. Therefore, the importance of the oxygen bulk diffusion in rate determination of the oxygen permeation process was gradually growing with the increase of operation temperature and a decrease in the overall E_a for oxygen permeation would be then observed. Between 850 and 900°C, an average E_a of 62.1 kJ mol^{-1} was observed. It therefore suggests that the E_a for bulk oxygen diffusion should be equal or less than 62.1 kJ mol^{-1}.

Conclusion

About 5 mol % of Sc^{3+} doping into the B-site of $SrCoO_{3-\delta}$ resulted in an effective phase transfer from the oxygen vacancy ordered and structurally distorted 2-H hexagonal perovskite to the oxygen vacancy disordered cubic perovskite structure. Such a phase transition substantially increased the electrical conductivity from only ~4 to ~180 S cm^{-1} at 300°C. Ultra high permeation flux was observed for the SSC membrane between 750–900°C, which are comparable with that reported highly permeable $Ba_{0.5}Sr_{0.5}Co_{0.8}Fe_{0.2}O_{3-\delta}$ and $SrCo_{0.8}Fe_{0.2}O_{3-\delta}$ membranes. The permeation process of SSC was found to be mainly rate-determined by the slow oxygen surface exchange kinetics at the air side membrane surface at reduced temperatures. To increase the oxygen permeation flux at lower temperatures, future work should be focused on the membrane surface modification, particularly at the air sweep side. The activation energy for oxygen surface exchange is around 126 kJ mol^{-1}, while the E_a for oxygen bulk diffusion is $\leq$62.1 kJ mol^{-1}.

Acknowledgments

Dr. Zongping Shao appreciates the start-up funding for research from Nanjing University of Technology. This works is also supported by the National Natural Science Foundation of China under Award No. 20646002 and Natural Science Foundation of JiangSu Province, P.R. China under Award No. BK2006180.

Notation

J_{O_2} = oxygen flux, mL · cm^{-2} · min^{-1}
I_{O_2} = current density, A
F = Faraday, 96,500 C
E_{s1} = chemical potential inputted at the surface of high oxygen partial pressure, V
E_{s2} = chemical potential inputted at the surface of low oxygen partial pressure, V
E_b = chemical potential inputted at the bulk, V
R_{s1} = the resistances to surface oxygen exchange at high oxygen partial pressure side, Ω
R_{s2} = the resistances to surface oxygen exchange at low oxygen partial pressure side, Ω
R_b = the resistances to surface oxygen exchange at bulk, Ω
T = operating temperature, K
R = gas constant, 8.314 J · mol^{-1} · K^{-1}
p'_{O_2} = oxygen partial pressure at the oxygen feed side atmosphere, Pa
p''_{O_2} = oxygen partial pressure at the oxygen sweep side atmosphere, Pa
$p'^{S}_{O_2}$ = oxygen partial pressure at the oxygen feed side membrane surface, Pa
$p''^{S}_{O_2}$ = oxygen partial pressure at the oxygen sweep side membrane surface, Pa
S = membrane surface area, m^2
V_m = mole volume of the oxide, m^3
$[V_o^{oo}]_S$ = oxygen vacancy concentration at the surface
σ_{ion} = oxygen ionic conductivity, S cm^{-1}
σ_e = electronic conductivity, S cm^{-1}
D_V = Effective diffusivity of oxygen vacancy, m^2 s^{-1}
σ^o_{ion} = oxygen ionic conductivity of the material at standard condition, S cm^{-1}
n = n the power of oxygen partial pressure, dimensionless

Literature Cited

1. Teraoka Y, Zhang H, Furukawa S, Yamazoe N. Oxygen permeation through perovskite-type oxides. *Chem Lett*. 1985;11:1743.
2. Stevenson JW, Armstrong TR, Carnein RD, Pederson LR, Weber WJ. Electrochemical properties of mixed conducting perovskites $La_{1-x}M_xCo_{1-y}Fe_yO_{3-\delta}$ (M=Sr, Ba, Ca). *J Electrochem Soc*. 1996; 143:2722.
3. Ishihara T, Yamada T, Arikawa H, Nishiguchi H, Takita Y. Mixed electronic-oxide ionic conductivity and oxygen permeating property of Fe-, Co- or Ni-doped $LaGaO_3$ perovskite oxide. *Solid State Ionics*. 2000;135:631.
4. Shao ZP, Xiong GX, Dong H, Yang WS, Lin LW. Synthesis, oxygen permeation study and membrane performance of a $Ba_{0.5}Sr_{0.5}Co_{0.8}Fe_{0.2}O_{3-\delta}$ oxygen-permeable dense ceramic reactor for partial oxidation of methane to syngas. *Sep Purif Technol*. 2001;25:97.
5. Ishihara T, Tsuruta Y, Todaka T, Nishiguchi H, Takita Y. Fe doped $LaGaO_3$ perovskite oxide as an oxygen separating membrane for CH_4 partial oxidation. *Solid State Ionics*. 2002;152/153:709.
6. Shao ZP, Dong H, Xiong GX, Cong Y, Yang WS. Performance of a mixed-conducting ceramic membrane reactor with high oxygen permeability for methane conversion. *J Membr Sci*. 2001;183:181.
7. Kharton VV, Yaremchenko AA, Kovalevsky AV, Viskup AP, Naumovich EN, Kerko PF. Perovskite-type oxides for high-temperature oxygen separation membranes. *J Membr Sci*. 1999;163:307.
8. Jin W, Li S, Huang P, Xu N, Shi J, Lin YS. Tubular lanthanum cobaltite perovskite-type membrane reactors for partial oxidation of membrane to syngas. *J Membr Sci*. 2003;166:13.
9. Elshof JET, Bouwmeester HJM, Verweij H. Oxidative coupling of methane in a mixed-conducting perovskite membrane reactor. *Appl Catal A*. 1995;130:195.
10. Zhu XF, Wang HH, Yang WS. Novel cobalt-free oxygen permeable membrane. *Chem Commun*. 2004;1130.
11. Lu H, Tong JH, Deng ZQ, Cong Y, Yang WS. Crystal structure, oxygen permeability and stability of $Ba_{0.5}Sr_{0.5}Co_{0.8}Fe_{0.1}M_{0.1}O_{3-\delta}$

(M=Fe, Cr, Mn, Zr) oxygen-permeable membranes. *Mater Res Bull*. 2006;41:483.
12. Fabbrini L, Kryukov A, Cappelli S, Chiarello GL, Rossetti I, Oliva C, Forni L. $Sr_{1-x}Ag_xTiO_{3\pm\delta}$ (x = 0, 0.1) perovskite-structured catalysts for the flameless combustion of methane. *J Catal*. 2005;232:247.
13. Wang CH, Chen CL, Weng HS. Surface properties and catalytic performance of $La_{1-x}Sr_xFeO_3$ perovskite-type oxides for methane combustion. *Chemosphere*. 2004;57:217.
14. Rida K, Benabbas A, Bouremmad F, Peña MA, Martínez-Arias A. Surface properties and catalytic performance of $La_{1-x}Sr_xCrO_3$ perovskite-type oxides for CO and C_3H_6 combustion. *Catal Commun*. 2006;7:963.
15. Balachandran U, Dusek JT, Maiya PS, Ma B, Mieville RL, Kleefish MS, Udovich CA. Ceramic membrane reactor for converting methane to syngas. *Catal Today*. 1997;36:265.
16. Hendriksen PV, Larsen PH, Mogensens M. Prospects and problems of dense oxygen permeable membranes. *Catal Today*. 2000;56:283.
17. Bouwmeester HJM. Dense ceramic membranes for methane conversion. *Catal Today*. 2003;82:141.
18. Teraoka Y, Zhang H, Okamoto K, Yamazoe N. Mixed ionic-electronic conductivity of $La_{1-x}Sr_xCo_{1-y}Fe_yO_{3-\delta}$. *Mater Res Bull*. 1988;23:51.
19. Wang HH, Tablet C, Feldhoff A, Caro J. Based on the perovskite-type oxide $Ba_{0.5}Sr_{0.5}Zn_{0.2}Fe_{0.8}O_{3-\delta}$. *Adv Mater*. 2005;17:1785.
20. Tong JH, Yang WS, Zhu BC, Cai R. Investigation of ideal zirconium-doped perovskite-type ceramic membrane materials for oxygen separation. *J Membr Sci*. 2002;203:175.
21. Shao ZP, Yang WS, Cong Y, Dong H, Tong JH, Xiong GX. Investigation of the permeation behavior and stability of a $Ba_{0.5}Sr_{0.5}Co_{0.8}Fe_{0.2}O_{3-\delta}$ oxygen membrane. *J Membr Sci*. 2000;172:177.
22. Pei S, Kleefish MS, Kobylinski TP, Faber J, Udovich CA, Zhang-Mccoy V, Dabrowski B, Balachandran U, Mieville RL, Poppel RB. Failure mechanisms of ceramic membrane reactors in partial oxidation of membrane to synthesis gas. *Catal Lett*. 1995;30:2001.
23. Bouwmeester HJM, Kruidhof H, Burggraaf AJ, Gellings PJ. Oxygen semipermeability of erbia-stabilized bismuth oxide. *Solid State Ionics*. 1992;53–56:460.
24. Qi XW, Lin YS. Electric conductivity and oxygen permeability of modified cerium oxides. *J Mater Sci*. 2003;38:1073.
25. Kharton VV, Viskup AP, Kovalevsky AV, Naumovich EN, Marques FMB. Ionic transport in oxygen-hyperstoichiometric phases with $KNiF_4$-type structure. *Solid State Ionics*. 2001;143:337.
26. Kruidhof H, Bouwmeester HJM, Doom RHEV, Burggraaf AJ. Influence of order–disorder transitions on oxygen permeability through selected nonstoichiometric perovskite-type oxides. *Solid State Ionics*. 1993;63:816.
27. Kharton VV, Kovalevsky AV, Tsipis EV, Viskup AP, Naumovich EN, Jurado JR, Frade JR. Mixed conductivity and stability of A-site-deficient $Sr(Fe,Ti)O_{3-\delta}$ perovskites. *J Solid State Electrochem*. 2002;7:30.
28. Wiik K, Aasland S, Hansen HL, Tangen LL, Ødegard R. Oxygen permeation in the system $SrFeO_{3-x}$–$SrCoO_{3-y}$. *Solid State Ionics*. 2002;152/153:675.
29. Kim S, Yang YL, Christoffersen R, Jacobson AJ. Oxygen permeation, electrical conductivity and stability of the perovskite oxide $La_{0.2}Sr_{0.8}Cu_{0.4}Co_{0.6}O_{3-x}$. *Solid State Ionics*. 1997;104:57.
30. Li SG, Jin WQ, Xu NP, Shi J. Mechanical strength, and oxygen and electronic transport properties of $SrCo_{0.4}Fe_{0.6}O_{3-\delta}$-YSZ membranes. *J Membr Sci*. 2001;186:195.
31. Zeng PY, Ran R, Chen ZH, Zhou W, Gu HX, Shao ZP, Liu SM. Efficient stabilization of cubic perovskite $SrCoO_{3-\delta}$ by B-site low concentration scandium doping combined with sol-gel synthesis. *J Alloys Compd*. In press.
32. Deng ZQ, Yang WS, Liu W, Chen CS. Relationship between transport properties and phase transformations in mixed-conducting oxides. *J Solid State Chem*. 2006;179:362.
33. Zener C. Interaction between the d-shells in the transition metals. II. Ferromagnetic compounds of manganese with perovskite structure. *Phys Rev*. 1951;82:403.
34. Ge L, Zhou W, Ran R, Shao ZP, Liu SM. Facile auto-combustion syntheses of $La_{0.6}Sr_{0.4}Co_{0.2}Fe_{0.8}O_{3-\delta}$ (LSCF) perovskite via a modified complexing sol–gel process with NH_4NO_3 as combustion aid. *J Alloys Compd*. In press.
35. Shao ZP, Xiong GX, Tong JH, Dong H, Yang WS. Ba effect in doped $Sr(Co_{0.8}Fe_{0.2})O_{3-\delta}$ on the phase structure and oxygen permeation properties of the dense ceramic membranes. *Sep Purif Technol*. 2001;25:419.
36. Qiu L, Lee TH, Liu LM, Yang YL, Jacobson AJ. Oxygen permeation studies of $SrCo_{0.8}Fe_{0.2}O_{3-\delta}$. *Solid State Ionics*. 1995;76:321.
37. Kharton VV, Viskup AP, Naumovich EN, Lapchuk NM. Mixed electronic and ionic conductivity of $LaCo(M)O_3$ (M=Ga, Cr, Fe or Ni) I Oxygen transport in perovskite $LaCoO_3$-$LaGaO_3$. *Solid State Ionics*. 1997;104:67.
38. Sammells AF, Schwartz M, Mackay RA, Barton TF, Peterson DR. Catalytic membrane reactors for spontaneous synthesis gas production. *Catal Today*. 2000;56:325.
39. Zeng PY, Chen ZH, Zhou W, Gu HX, Shao ZP, Liu SM. Re-evaluation of $Ba_{0.5}Sr_{0.5}Co_{0.8}Fe_{0.2}O_{3-\delta}$ perovskite as oxygen semi-permeable membrane. *J Membr Sci*. 2007;291:148.
40. Adler SB. Factors governing oxygen reduction in solid oxide fuel cell cathodes. *Chem Rev*. 2004;104:4791.

Manuscript received Jan. 8, 2007, and revision received Sept. 10, 2007.